**Title** : Measurement and inversion strategies for 3-D resistivity surveys with vector arrays

**Short running title** : Inversion strategies for 3-D surveys with vector arrays

**Authors** : Meng Heng Loke[1*], Paul B. Wilkinson[2], Julien Gance[3], Jean-Philippe Malet[4], Catherine Truffert[3], Orlando Leite[3]

[1] Geotomo Software Sdn Bhd, 115 Cangkat Minden Jalan 5, 11700 Gelugor, Penang, Heights, Malaysia.

Email ; drmhloke@yahoo.com

[*] Corresponding author

[2] British Geological Survey, Keyworth, Nottingham, NG12 5GG, U.K.

Email : pbw@bgs.ac.uk

[3] Iris Instruments,

Emails : j.gance@iris-instruments.com, c.truffert@iris-instruments.com, o.leite@iris-instruments.com

[4] CNRS / EOST – École et Observatoire des Sciences de la Terre, (Strasbourg, France)

Email : jeanphilippe.malet@unistra.fr

## Abstract

Three-dimensional geoelectrical surveys are widely used to map the subsurface in areas with complex geology. Field survey methods using the offset pole-dipole and dipole-dipole arrays have been proposed to map large areas efficiently. However, it has been found that negative apparent resistivity values are sometimes encountered in areas with large resistivity contrasts, particularly when large offsets between the current electrodes and potential dipoles are used. The vector array configuration that makes two measurements of the electric field at each station with two potential dipoles at right angles avoids this problem. The combined potential measured at the two dipoles is independent of the orientation the current electrodes to the receiver station. The amplitude of the vector apparent resistivity value is always positive. A commonly used configuration is to lay out the current and potential electrodes along alternating parallel lines. We examine the use of different offsets between the current electrodes and potential dipoles to improve the survey spatial resolution. A new inversion method using both the amplitude and direction of the vector array potentials is described to improve the resolution. Results from the inversion of a synthetic model data set and a field survey over a deep-seated landslide are shown.

**Data Availability Statement**

The data that support the findings of this study are available from the corresponding author upon reasonable request.

**Conflict of Interest Statement**

**Introduction**

3-D geoelectrical surveys are widely used to map the subsurface in areas with complex geology (White *et al.* 2001; Loke *et al.* 2013). New field survey techniques, such as the offset pole-dipole and dipole-dipole arrays with the current and potential electrodes arranged in alternating parallel lines, were designed to map large areas efficiently (Collins and White 2007). Some surveys use potential lines at a larger offset from the current lines to increase the survey depth but it sometimes results in array configurations with very low potential signals. In some cases, negative apparent resistivity values are obtained, particularly when there are large resistivity contrasts (Lee *et al.* 2014). Different situations where negative apparent resistivity values can occur are discussed in Wilkinson *et al.* (2008), Jung (2009), Jung *et al.* (2009) and Deidda *et al.* (2011). The logarithms of the apparent resistivity and the model resistivity are commonly used as the data and model parameters in inversion routines due to the large range of values that can occur in a data set (Johansen 1977), but it cannot be used if negative apparent resistivity values are present.

The vector array configuration was proposed by Zonge (1994) for carrying carry out surveys over large areas rapidly. At each receiver station, three potential electrodes that measure the electric field in two perpendicular directions are used. Similar tensor array configurations using perpendicular current dipoles have also been used (Risk *et al.* 1970; Doicin 1976; Keller and Furgerson 1977; Bibby and Risk 1992). New field survey instruments have made it practical to use such array configurations for detailed surveys (Truffert *et al.*

2019). Conventional inversion techniques that treat the two measurements as separate apparent resistivity data points cannot be used as some of them might have very high (or even infinite) geometric factors and be very sensitive to noise. In this paper, we propose a new method that combines the measurements into amplitude and direction components that are used as the data parameters in the inversion scheme. In the following section, we give a brief overview of the smoothness-constrained least-squares optimisation method and the use of vector arrays in modern surveys. This is followed by a description of the proposed inversion scheme that uses the amplitude and direction components derived from the vector array data set. Finally, we discuss the results using data sets from a synthetic model and a field survey over a deep-seated landslide.

**Method**

**Least-squares inversion method**

In the inversion of geoelectrical data, we seek to find a subsurface resistivity model so that the calculated apparent resistivity values match the measured values subject to constraints imposed on the model. A nonlinear optimisation method is usually used to find the minimum of an objective function $\Phi(\mathbf{r})$ such as that given below.

$$\Phi(\mathbf{r}) = \Phi_{\mathbf{d}}(\mathbf{r}) + \lambda \Phi_{\mathbf{s}}(\mathbf{r}) \tag{1}$$

**r** is a vector with the model resistivity values. $\Phi_d$ is a measure of the difference between the measured and calculated apparent resistivity values, while $\Phi_s$ is a measure of the model roughness (Oldenburg and Li 1994; Farquharson and Oldenburg 1998). $\lambda$ is the damping factor (Farquharson and Oldenburg 1998; Loke *et al.* 2013) that gives the relative weight given to reduce the model roughness compared to the data misfit.

The smoothness-constrained least-squares optimisation method is widely used in 2-D and 3-D resistivity and IP data inversion (Loke *et al.* 2013). The method usually converges rapidly to an acceptable solution. It has been used for inversion of data sets with several hundred thousand data points and model parameters using commonly available and inexpensive PCs (Loke *et al.* 2020). The following equation is used in an iterative manner to refine an initial model (frequently a homogeneous model) to determine the change in the model parameters (**Δr**) that will reduce the data misfit (**g**).

$$\left[\mathbf{J}_i^T \mathbf{R}_d \mathbf{J}_i + \lambda_i \mathbf{W}^T \mathbf{R}_m \mathbf{W}\right]\Delta\mathbf{r}_i = \mathbf{J}_i^T \mathbf{R}_d \mathbf{g}_i - \lambda_i \mathbf{W}^T \mathbf{R}_m \mathbf{W}\left(\mathbf{r}_{i-1} - \mathbf{r}_m\right) \tag{2}$$

The Jacobian matrix **J** contains the sensitivities of the (logarithm of) apparent resistivities with respect to the (logarithm of) the model resistivity values **r**. $\mathbf{r}_m$ is a reference model, while **W** is the roughness filter that minimises the change in the resistivity value across neighbouring model cells.  The above equation is solved to determine the change in the model parameters (**Δr$_i$**) that will reduce the data misfit **g$_i$**. **r$_{i-1}$** is the model from the previous iteration. **R$_d$** and **R$_m$** are weighting matrices used by the L1-norm inversion method (Farquharson and Oldenburg 1998) applied to the data misfit and model roughness. The data misfit **g** contains the difference between the logarithm of the measured and calculated apparent resistivity values.

**Vector arrays and transformation of data values**

Figure 1a shows a schematic diagram for a typical offset pole-dipole survey layout (White *et al.* 2001) with the current and potential electrodes arranged in alternating lines. This layout was designed for resistivity and IP surveys used to map mineral deposits at depths of up to several hundred metres. Large electrode spacings of 50 to 200 metres are commonly used covering survey areas of several square kilometres. Measurements are usually made between the current and potential electrodes in adjacent lines (a single offset measurement). In an effort to increase the depth of investigation with a limited number of lines, some surveys attempt to use potential lines at a larger offset from the current lines. This sometimes results in array configurations with very low potential signals, and in some cases even with negative apparent resistivity values, particularly when there are large resistivity contrasts (Lee *et al.* 2014). The logarithm of the apparent resistivity is frequently used as the data parameter in inversion schemes as it reduces the data values from a logarithmic to a linear range. It was shown by Johansen (1977) that using the logarithm of the apparent resistivity and model resistivity improved the convergence of the inversion method. However, it is not possible to use the logarithm for the data parameter if negative apparent resistivity values are present (Jackson *et al.* 2001). In such cases, it is necessary to use the apparent resistivity values as the data parameter. As they have a much larger range than the logarithms, a weighting scheme has to be used to avoid a situation where excessive weight is given to reducing the data misfit for data points with large apparent resistivity values. In some field surveys, a situation may arise where the current electrode is located

exactly in between the potential electrodes (Figure 1b). This results in an array configuration with an infinite geometric factor where the apparent resistivity value is undefined.

Figure 1c shows a possible layout using the vector array configuration (Loke *et al.* 2019; Truffert *et al.* 2019). In many surveys, the second current electrode (C2) is at a fixed location that is sufficiently far away so that its effect on the measured potential is small and can be neglected. Instead of two potential electrodes, each receiver station has three electrodes, with a common positive P1 electrode and two negative P2 electrodes. Ideally, the P1-P2$_a$ and P1-P2$_b$ dipoles are perpendicular to each other. At each receiver station two resistance values are measured ($r_a$ and $r_b$) associated with the potential dipoles P1-P2$_a$ and P1-P2$_b$ (Figure 2). The values of the individual resistance components vary with the orientation of the potential dipoles with respect to the current electrode (Figure 2). However, it avoids a situation where a resistance value of zero is measured at both dipoles. For example, in Figure 2a, the current electrode C1 is almost at the middle point of the P1-P2$_b$ potential dipole. This will result in a very small resistance value as measured by this dipole. In comparison, the P1-P2$_a$ is almost colinear with the C1 electrode, so the measured resistance value will be much larger. Figure 2b shows a situation where a small resistance value will be measured at the P1-P2$_a$ potential dipole but a larger value at the P1-P2$_b$ dipole. Regardless of the orientation of the current electrode with respect to the dipoles, at least one of the dipoles will have a non-zero resistance value.

Figure 3 shows a schematic diagram of a vector array measurement with two resistance components. Ideally the angle $\gamma$ between the two arms (P1-P2$_a$ and P1-P2$_b$) of the vector array potential electrodes should be 90 degrees. However, in many field surveys it usually

varies between 80 to 100 degrees. The two vectors ($\mathbf{r_a}$ and $\mathbf{r_b}$) can be combined into a single vector $\mathbf{r_c}$ (Figure 3a) as follows:

$$\mathbf{r_c} = [r_a \sin(\alpha) + r_b \sin(\beta)].\mathbf{i} + [r_a \cos(\alpha) + r_b \cos(\beta)].\mathbf{j} \ ,$$

where $\mathbf{i}$ and $\mathbf{j}$ are unit vectors in the $x$ and $y$ directions. The amplitude of the combined vector is then given by

$$r_c = \left[(r_a \sin(\alpha) + r_b \sin(\beta))^2 + (r_a \cos(\alpha) + r_b \cos(\beta))^2\right]^{0.5} = \left[r_a^2 + r_b^2 + 2r_a r_b \cos(\beta - \alpha)\right]^{0.5},$$

which can be simplified to

$$r_c = \left[r_a^2 + r_b^2 + 2r_a r_b \cos(\gamma)\right]^{0.5}. \tag{3}$$

To convert the resistance amplitude $r_c$ to an apparent resistivity value, we derive the equation for the corresponding geometric factor term. For a homogeneous half-space with resistivity $\rho$, the relationship between the measured resistance and the geometric factor can be written as follows:

$$r_a = \rho.k_a, \ r_b = \rho.k_b \ .$$

$k_a$ and $k_b$ are reciprocals of the geometric factors associated with the two components of the vector array. Substituting the relationships into equation (3), we get:

$$\rho.k_c = \left[(\rho.k_a)^2 + (\rho.k_b)^2 + 2\rho.k_a \rho.k_b \cos(\gamma)\right]^{0.5}, \text{ which leads to}$$

$$k_c = \left[k_a^2 + k_b^2 + 2k_a k_b \cos(\gamma)\right]^{0.5}, \tag{4}$$

with $k_c$ being the reciprocal of the geometric factor for the amplitude resistance component $r_c$. The apparent resistivity amplitude value ($\rho_c$) can then be calculated by the following equation:

$$\rho_c = Kr_c, \text{ where } K = 1/k_c \ . \tag{5}$$

Using the amplitude of the vector potentials avoids the problem of very high geometric factors and noisy data when a potential dipole is almost on an equipotential line. The geometric factor for the amplitude is always smaller than (or at most equal to) the smallest geometric factor of the individual components. To verify equations (3) and (5) are correct, calculations were carried out for a homogeneous half-space where the apparent resistivity value should be the same as the model resistivity.

The least-squares equation (2) includes the Jacobian matrix **J** that contains the partial derivative of the logarithm of the apparent resistivity with respect to the logarithm of the model resistivity. The partial derivative of the resistance amplitude $r_c$ can be calculated from the partial derivatives of the individual components using the following relationship.

$$\frac{\partial r_c}{\partial \rho_j} = \frac{r_a + r_b \cos(\gamma)}{r_c} \cdot \frac{\partial r_a}{\partial \rho_j} + \frac{r_b + r_a \cos(\gamma)}{r_c} \cdot \frac{\partial r_b}{\partial \rho_j} \tag{6}$$

$\rho_j$ is the resistivity of the $j$th model cell. The partial derivatives of the individual components $r_a$ and $r_b$ are calculated using the adjoint-equation method (McGillivray and Oldenburg 1990). In the vector array layout (Figure 1c), a number of potential measurements are made using the same current electrode. A fast method to calculate the partial derivatives with the finite-element method is described in Loke *et al.* (2020). Using the amplitude component alone has the advantage that inversion algorithms designed for processing apparent resistivity data from conventional arrays can be easily adapted for vector array data (Loke *et al.* 2019). The average of the amplitude apparent resistivity values is used to set the initial homogenous model for the smoothness-constrained least-squares method if there is no

prior information about the subsurface resistivity. However, using the amplitude component alone does not make full use of the data available.

A single vector array measurement has two independent readings, $r_a$ and $r_b$. Thus, the transformed measurement should also have two values, the amplitude and a direction component. If the *x*-axis in Figure 3a is used as reference direction, the direction of the combined resistance values is the angle θ. So, theoretically the direction can be used as a second data parameter for the inversion. However, one disadvantage of using the angle as a data parameter is that it is not a continuous variable. For example, the configuration shown in Figure 3b gives a combined vector with a small positive angle θ with respect to the *x*-axis. A small shift in the position of the C1 electrode will result in a negative value for the $r_b$ component such that the $r_c$ vector is now below the *x*-axis. If the convention that angles have a range of 0 to 2π is used, the angle (measured in the anti-clockwise direction from the *x*-axis) in Figure 3c will now be 2π-θ. This results in a discontinuity in the angle value for a small change in the $r_b$ component. The least-squares method makes use of the Jacobian matrix that contains the partial derivative of the data parameter with respect to the model resistivity value, so ideally the data parameter should be a continuous variable. In array configurations with large geometric factors, a change in the model resistivity near the electrodes can cause the calculated resistance value to change from positive to negative. For the vector array, this would cause a corresponding change in the direction component from θ to 2π-θ. In this paper, a data parameter that contains the angle information as a continuous variable is used. We use the ratio of the first ($r_a$) resistance component to the amplitude resistance value as follows:

$$d_c = r_a / r_c .$$ (7)

In the ideal setup with the two potential dipoles at right angles, this is equals to the cosine of the angle θ between the combined vector $r_c$ and the $r_a$ component (Figure 3b). The partial derivative of this parameter with respect to the model cell resistivity $\rho_j$ is given below:

$$\frac{\partial d_c}{\partial \rho_j} = \frac{1}{r_c}\left[\frac{\partial r_a}{\partial \rho_j} - \frac{r_a}{r_c}\frac{\partial r_c}{\partial \rho_j}\right].$$
(8)

The direction component $d_c$ has values ranging from -1 and +1, or a maximum range of 2. The range of values for the logarithm of the apparent resistivity values is dependent on the data set. If both the amplitude and direction components are used in the data parameter vector, then the data misfit term in equation (1) can be written as

$$\Phi_d(\mathbf{r}) = \Phi_{da}(\mathbf{r}) + w\Phi_{dd}(\mathbf{r}),$$
(9)

with $\Phi_{da}$ and $\Phi_{dd}$ being the data misfit terms for the amplitude and direction data components, and $w$ being the relative weight given to the direction component. The ranges of the two components are used to set the relative weight $w$. For example, if the apparent resistivity values vary from 1 to 100, the range of the logarithm of the resistivity values is 4.6. The weight is then set at 2.3 (i.e. 4.6/2.0) so that the contributions of both components to the data misfit term are approximately the same.

An alternative inversion method was proposed by Jackson (2001) that uses the electric field as the data parameter instead of the apparent resistivity. An approximation of the electric field is calculated from the potential difference measured by the potential dipole divided by the dipole length. This approximation is usually considered sufficiently accurate if the dipole length is less than one-fifth the distance of the current electrode to the nearest potential electrode (Keller and Frischknecht 1966). In some field data sets (Loke *et al.* 2019), the distance between the current and potential electrodes is less than the potential dipole

length for some of the data points. Thus, using the approximation for calculating the electric field is not sufficiently accurate for these data points. The vector array approach does not have this limitation as the resistance values are used.

**Results**

In this section we show results of tests conducted with a synthetic resistivity model and a field data set acquired over a deep-seated landslide.

**Synthetic data set**

Figure 4a shows the arrangement of the electrodes used to generate the synthetic data set. The test model used has six rectangular blocks embedded in a 50 Ω.m background medium (Figure 4b). The pole-dipole array is used where the second current electrode is assumed to be sufficiently far from the survey grid so that it's effect can be neglected. The current electrodes are located along seven lines in the *x*-direction, while the potential electrodes triplets are arranged along four lines between the current lines. In generating the test data set, we put a restriction that the distance of a current electrode from the P1 electrode in the array used does not exceed 20 times the potential dipole length (1 m in this example) to ensure that potential signal is not too low. For the first data set, we use arrays where the vector potential triplets are located next to the current line. For example, the current electrodes located along *y* equals to 4 m use the potential triplets at *y* equals to

2.25-3.32 and 5.25-6.25 m. This generates a vector array data set with 2870 measurements. The second data set includes measurements with the potential dipoles up to two potential lines away that gives a data set with 5138 data points. Similarly, the third data set includes the potential triplets up to four potential lines away from the current electrode giving a data set with 7842 data points. The final data set uses the offset pole-dipole array (with the potential dipoles aligned in the *x*-direction) with a single potential line offset. The data set has 2870 measurements but two data points with negative apparent resistivity values were removed. Increasing the offset of the potential lines significantly increases the number of data points with negative apparent resistivity values. Thus, the offset pole-dipole with only a single offset is used. Gaussian random noise with an amplitude of 1 mΩ was added to the resistance values. This resulted in an average error of about 1.2% in the apparent resistivity values for the offset pole-dipole and vector arrays with single and double offsets (with differences of less than 0.05%). The vector array data set with quadruple offset has a slightly higher noise level of 1.4%, probably because it has more data points with longer offsets.

In the inversion of the data sets, the L1-norm was used for both the data misfit and model roughness (Farquharson and Oldenburg 1998). The data misfit was calculated using the average of the absolute difference between the logarithms of the measured and calculated apparent resistivity values. Since the true model resistivity values are known for the synthetic model, the difference between the true and inverse model resistivity values can be used to assess the accuracy of results using the following equation.

$$\partial_a = \left[ \sum_1^m |\partial(j)| \right] / m, \text{where } \partial(j) = 100.[r_t(j) - r_m(j)] / r_t(j) \tag{7}$$

$m$ is the number of model cells. $r_t$ is the true model resistivity, while $r_m$ is the inverse model resistivity. The model resolution $\mathbf{M_R}$ (Menke 1984; Day-Lewis *et al.* 2005) for the different data sets is also calculated using the following equation.

$$\mathbf{M_R} = \left[\mathbf{J_i^T R_d J_i} + \lambda_i \mathbf{W^T R_m W}\right]^{-1}\left[\mathbf{J_i^T R_d J_i}\right]$$  (8)

The diagonal elements of the $\mathbf{M_R}$ matrix give the resolution values of the model cells. The resolution values are limited to between 0.0 (for no resolution) and 1.0 (for perfect resolution). To reduce the resolution information into a single number, we calculate average of the resolution values. The results from the inversion of the different data sets with the data misfit, model misfit and average resolution values are summarised in Table 1.

The inverse models obtained for the offset pole-dipole and vector arrays (where only the amplitude component is used) are shown in Figure 5. The inverse model used has 9 layers and a total of 5832 cells. Only the top eight layers are shown as the last layer does not show significant variations in the resistivity values. The results obtained with the offset pole-dipole and the vector array with a single offset are fairly similar. The vector array inverse model has a lower model misfit but the offset pole-dipole model has a higher average resolution. The shape of the anomalies in the offset pole-dipole array model are slightly elongated in the *y*-direction as the potential dipoles are always aligned in the *x*-direction which causes a slight directional bias in the data. Increasing the maximum offset allowed for the vector array to two potential lines results in a significantly lower model misfit and higher average resolution value (Table 1) compared to the data set with a single offset. The larger high resistivity block in layers 2 and 3, as well as the large low resistivity block in layers 4 to 6, are significantly better resolved in the double offset vector array inverse model (Figure

5c) compared to the single offset model (Figure 5b). Increasing the maximum offset allowed to four potential lines does not seem to improve the results. The average model resolution is slightly higher compared to the double offset data set (Table 1), but the data and model misfits are also slightly higher. This is probably because the benefit of having more data points is negated by the increase in the data noise level due to the arrays with larger distances between the current and potential electrodes.

The results obtained when both the vector array amplitude and direction components are used in the data set are shown in Figure 6 and listed in the lower half of Table 1. The model for the single offset vector array data set has a significantly lower model misfit and higher average resolution compared to the model where only the amplitude component was used. Similar improvements are observed with the double and quadruple offsets vector array data sets. The best inverse model is again obtained by the double offset vector array data set in terms of the model misfit (Table 1). This result could be used in planning field surveys where a large area needs to be mapped by a limited number of potential receivers. A roll-along procedure could be used by laying out two potential lines at a time since taking readings with more than two offset lines at a time does not seems to significantly improve the results.

Figure 7 shows the model resolution sections for the different model layers as the number of offsets is increased and the addition of the direction component to the data set. The model resolution decreases exponentially with depth. There are lateral variations due to changes in the model resistivity, such as the higher resolution values at the deeper low resistivity block in layers 4 to 6. Increasing the offset from 1 to 2 results in a significant

increase in the resolution values, particularly in layers 3 to 5 (Figures 7a and 7b). Adding the direction component causes an additional increase in the resolution values (Figures 7c).

**Field data set**

This survey was conducted by IRIS Instruments and EOST (France) in the French Pyrénées, at the recently reactivated Viella landslide (Gance *et al.* 2021). General information on landslides in the Pyrénées region and geology of the area can be found in Bernardie *et al.* (2021) and Batailles and Lespine (2019). The Viella slope is composed of a complex mixture of sedimentary material associating torrential deposits, moraine deposits (from the Bastan ice glacier), colluvium, screes and weathered blocks of shales from previous historical rockfalls triggered from the overhanging cliff. The few boreholes drilled (up to 71 m in depth) did not reach the bedrock. The interpretation of several 2-D ERT profiles carried out in the area showed a very heterogeneous geology in the subsurface, from 0 to - 40 m. The resistivities of the media vary from 20 to 3000 Ω.m, depending strongly on the water content but also on the proportion of shale blocks and sandy-gravel matrix. The survey was conducted to propose a representative 3-D model of the entire slope from the surface to a depth of 250 m in order to identify large-scale structures controlling the mechanics of the landslide, and to characterize the properties of the water reservoir that was not possible from the shallow high-resolution ERT.

A satellite map of the survey area is shown in Figure 8a, while Figure 9 shows the survey layout with the positions of the electrodes. The main survey area is on the western half where most of the electrodes are located. There is a prominent gap in the area covered by the electrodes at the location of the Viella village. Two locations were used for the remote second current electrode. The finite element mesh was extended to include the

remote electrodes so their effects could be accurately calculated. The distances of the remote electrodes are not sufficiently far such that their effects can be neglected.

If the data is processed as conventional 4-electrodes arrays, it gave a number of negative apparent resistivity values with geometric factors ranging from 90 to 1.9 billion m. Thus, it is not possible to use logarithm of the apparent resistivity values as the data parameter. The absolute values of the apparent resistivity values range from to about 5 to 90,000 Ω.m, or a ratio of about 18,000 between the highest and lowest values. The resistance values range from 0.0004 to 3.0 Ω (ratio of 75,000). The least-squares method attempts to minimise the difference between the calculated and measured data values. It gives a greater weight to the data values with the larger amplitudes if the apparent resistivity or resistance is used as the data parameter. This effect can be reduced by constructing a data weighting matrix, $\mathbf{R_d}$ in equation (2), so that different data points are given approximately equal weights. The resulting inverse model would then be partly dependent on the choice of the data weighting matrix. When converted to vector amplitude values, the apparent resistivity values have a much smaller range of 9 to 2430 Ω.m, or 2.2 to 7.8 (ratio of 3.5) when the logarithm is used. The direction values have fixed limits of -1.0 to 1.0. The vector amplitude and direction values have a much smaller range than the original resistance or apparent resistivity values.

The inverse models obtained using the amplitude component only, and with also the direction component included, are shown in Figure 10. We use the approach by Haber *et al.* (2007) where the inversion process starts with a large damping factor which is slowly reduced after each iteration. This results in a more stable inversion algorithm. The output from the inversion algorithm using a slow cooling damping sequence is a series of inverse

models each with its own data misfit and model roughness. The L-curve method (Farquharson and Oldenburg 2004) was then used as a post-inversion tool to select the model with the optimum balance between the data misfit and model roughness. Figure 11a shows a plot of the model roughness versus the data misfit from the inversion of the data set using the amplitude only. As the damping factor is reduced, the data misfit is reduced while the model roughness increases. Figure 11b shows a plot of the curvature of the L-curve that has a maximum for the inverse model with a data misfit of 10.2% which is selected as the model shown in Figure 10a. The same method is used to select the optimum inverse model (with a data misfit of 9.1%) using the amplitude and direction data.

The high resistivity zones of above 300 $\Omega$.m (in Figures 10a and 10b) correspond to known limestone formations. There is an interesting low resistivity feature in the bottom five layers of the models towards the left section of the survey area that might indicate a fracture zone with higher water content that could act as a landslide reservoir and trigger. The region with the conductive anomaly is overlain by a dejection cone of reworked materials created by rockfalls from an overhanging scarp (Figure 8b). The cone of rockfalls material appears as a high resistivity band above the conductive anomaly (Figure 12). The low resistivity feature is more prominent in the inverse model that also uses the direction component. This is due to the improvement in the model resolution when the direction component is included in the data set. Drilling has been planned to identify the nature of the low resistivity zone.

**Discussion**

Tests with a synthetic model and a field data set show that converting the vector array measurements into amplitude and direction components has been successful in inverting the data sets. Not surprisingly, including the direction component in the data set improved the resolution of the inverse model compared to using the amplitude component alone. The optimum inverse model that balances the data misfit with the model roughness can be determined by using a post inversion L-curve procedure.

The ratio of the first resistance component ($r_a$) to the amplitude resistance value ($r_c$) was used for the direction component. The amplitude component $r_c$ has contributions from both the $r_a$ and $r_b$ components. Thus, the direction parameter $d_c$ has information from both components, although it is possible that slightly more weight is given to the $r_a$ component as it occurs in both the numerator and denominator of $d_c = r_a/r_c$. One possible alternative is to use the ratio of the components, such as $r_a/r_b$ if $r_b$ has a larger amplitude (and similarly $r_b/r_a$ if $r_a$ has a larger amplitude to avoid instability) for each data point. Another possibility is to use ($r_b/r_c$) for the direction component for data points where $r_b$ has a larger amplitude. These refinements of the inversion algorithm are being investigated.

The tensor array (Risk *et al.* 1970; Zonge 1994) uses a similar configuration with two perpendicular potential dipoles but also with two perpendicular current dipoles. The data from each tensor measurement can be separated into two vector array measurements and the data set processed using the vector array inversion algorithm. Bibby (1977, 1986) proposed the use of the 'apparent resistivity tensor'. Several invariant parameters were derived from the apparent resistivity tensor in an attempt to identify boundaries and other subsurface parameters from field measurements. Bibby (1986) demonstrated the use of the

tensor invariant parameters using simple models such as a horizontally layered medium, vertical contact and a hemispherical sink. The simple models were used due to limited computational resources available at that time. However, they have limited applications for field data sets collected over more complex structures. However, the 'apparent resistivity tensor' concept could be an interesting alternative to the amplitude and direction parameters in the least-squares inversion algorithm for tensor array surveys using modern numerical techniques and computing facilities. This is an area that requires further research.

**Conclusion**

The use of both the amplitude and direction components of the vector array measurements improves the model spatial resolution compared to using the amplitude component only. It makes full use of the information available in the data set. Transforming the measured resistance values into the amplitude and direction components makes them less sensitive to noise. The post-inversion L curve method using a slow cooling sequence for the damping factor is a stable inversion algorithm. The optimum inverse model that balances a low data misfit while minimising artifacts due to noise can be estimated by using a post-inversion L-curve procedure.

Tests currently carried out with IP data sets (Loke *et al.* 2019) show a similar improvement in the resolution of the IP inverse model when the direction component is also used. A homogenous initial model (using the average of the amplitude apparent resistivity values) is currently used for the inversion algorithm. We are also studying whether the use of a non-homogeneous initial model calculated using the Born approximation method (Li and Oldenburg 1992) will improve the convergence of the least-squares inversion method. Research is also being carried out on the use of the resistance or electric field values directly as the data parameter for the inverse algorithm,

particularly for arrays such as the offset pole-dipole and dipole-dipole arrays where it is not possible to convert the measurements into amplitude and direction values.

**ORCID**

*Meng Heng Loke* ID https://orcid.org/0000-0003-4935-8014

**References**

Batailles, C. and Lespine, L. (2019) Etude de Bassin de Risque de la Division Domaniale de Viella (Haute-Pyrénées, France). Office National des Forêts - Service de Restauration des Terrains de Montagne, Tarbes, France, 322p.

Bernardie, S., Vandromme, R., Thiery, Y., Houet, T. Grémont, M., Masson, F., Grandjean, G. and Bouroullec, I. (2021) Modelling landslide hazards under global changes: the case of a Pyrenean valley. *Nat. Hazards Earth Syst. Sci.*, 21, 147–169.

Bibby, H. M. (1977) The apparent resistivity tensor. *Geophysics*, 42, 1258-1261.

Bibby, H. M. (1986) Analysis of multiple-source bipole-quadripole resistivity surveys using the apparent resistivity tensor. *Geophysics*, 51, 972-983.

Bibby, H.M. and Risk, G.F. (1992) Influence of large-scale resistivity setting on interpretation of resistivity within geothermal areas. *Proc. 14th New Zealand Geothermal Workshop* 1992, 223-230.

Collins, S. and White, R.M.S. (2007) Six years experience with Offset pole-dipole and other 3D IP arrays. What have we learnt? *ASEG Extended Abstracts* 2007(1), 1–4.

Day-Lewis, F.D., Singha, K. and Binley, A. (2005) The application of petrophysical models to radar and electrical resistivity tomograms: resolution dependent limitations. *Journal of Geophysical Research*, 110, B08206.

Deidda, G.P., Mura, M. and Schirru, F. (2011) Negative Apparent Resistivity and Chargeability in Crosshole Electrical Surveys. *73rd EAGE Conference & Exhibition*, Vienna, Austria, 23-26 May 2011, P188.

Doicin, D. (1976) Quadripole-quadripole arrays for direct current resistivity measurements -Model studies. *Geophysics*, 41, 79-95.

Farquharson, C.G., and Oldenburg, D.W. (1998) Nonlinear inversion using general measures of data misfit and model structure. *Geophysical Journal International*, 134, 213-227.

Farquharson, C.G., and Oldenburg, D.W. (2004) A comparison of automatic techniques for estimating the regularization parameter in non-linear inverse problems. *Geophysical Journal International*, 156, 411-425.

Gance, J., Leite, O., Lajaunie, M., Susanto, K., Truffert, C., Maillard, O. and Malet, J. P. (2021) Dense 3D electrical resistivity tomography to understand complex deep landslide structures. *EGU General Assembly Conference Abstracts* (pp. EGU21-14522).

Haber, E., Oldenburg, D.W. and Shekhtman, R. (2007) Inversion of time domain three-dimensional electromagnetic data. *Geophysical Journal International*, 171, 550–564.

Jackson, P.D., Earl, S.J. and Reece, G.J. (2001) 3D resistivity inversion using 2D measurements of the electric field. *Geophysical Prospecting*, 49, 26-39.

Johansen, H.K. (1977) A man/computer interpretation system for resistivity soundings over horizontally stratified earth. *Geophysical Prospecting*, 25, 667–691.

Jung, H., (2009) Negative Apparent Resistivity Effect by a Steel Casing Borehole Near Electrical Dipole-Dipole Survey Line. *Near Surface 2009–15th European Meeting of Environmental and Engineering Geophysics*, Dublin, Ireland, 7-9 September 2009, A39.

Jung, H.K., Min, D.J., Lee, H.S., Oh, S.H. and Chung, H.J. (2009) Negative apparent resistivity in dipole–dipole electrical surveys. *Exploration Geophysics*, 40, 33-40.

Keller, G.V. and Frischknecht F.C. (1966) *Electrical methods in geophysical prospecting*. Pergamon Press Inc., Oxford.

Keller, G. V. and Furgerson, R. B. (1977) Determining the resistivity of a resistant layer in the crust. *Am. Geophys. Union Geophysics Monograph* X, 440-469.

Lee, H., Jung, H.K., Cho, S.H. and Min, D.J. (2014) Negative Apparent Resistivity in 2.5D Dipole-dipole Electrical Survey for a Very Simple Model. *Near Surface Geoscience 2014*, 20th European Meeting of Environmental and Engineering Geophysics.

Li, Y. and Oldenburg, D. W. (1992) Approximate inverse mappings in DC problems. *Geophysical Journal International*, 109, 343 - 362.

Loke, M.H., Chambers, J.E., Rucker, D. F., Kuras, O. and Wilkinson, P. B. (2013) Recent developments in the direct-current geoelectrical imaging method. *Journal of Applied Geophysics*, 95, 135-156.

Loke, M.H., Gance, J., Truffert, C. and Leite, O. (2019) The inversion of vector array data sets for 3-D resistivity and I.P. surveys. *Near Surface Geoscience Conference & Exhibition 2019*, 8-12 September 2019, The Hague, Netherlands, Mo_25th_A11.

Loke, M.H., Papadopoulos, N, Wilkinson, P.B., Oikonomou, D., Simyrdanis, K. and Rucker, D. (2020) The inversion of data from very large 3-D ERT mobile surveys. *Geophysical Prospecting*, 68, 2579-2597.

McGillivray P.R. and Oldenburg D.W. (1990) Methods for calculating Fréchet derivatives and sensitivities for the non-linear inverse problem: a comparative study. *Geophysical Prospecting*, 38, 499-524.

Menke, W. (1984) *Geophysical data analysis : Discrete inverse theory*. Academic Press Inc.

Oldenburg, D.W. and Li, Y. (1994) Inversion of induced polarization data. *Geophysics*, 59, 1327-1341.

Risk, G. F., Rayner. H. H., Stagpoole, V. M., Graham, D. J., Dawson, G. B. and Bennie, S. L. (1984) Electrical resistivity survey of the Wairakei geothermal field. *Geophysics Div. Rep. no. 200*, Dept. of Scientific and Industrial Research, Wellington.

Truffert, C., Loke, M.H., Arce, J., Gance, J. and Leite, O. (2019) Benefits of new equipment's and inversion code for full- 3D DC resistivity and IP surveys: example from South-America. *Extended Abstracts-16th SAGA Biennial Conference & Exhibition 2019*, Durban, South Africa.

White, R.M.S., Collins, S., Denne, R., Hee, R. and Brown, P. (2001) A new survey design for 3D IP modelling at Copper Hill. *Exploration Geophysics*, 32, 152-155.

Wilkinson, P. B., Chambers, J. E., Lelliot, M., Wealthall, G. P. and Ogilvy, R. D. (2008) Extreme sensitivity of crosshole Electrical Resistivity Tomography measurements to geometric errors. *Geophysical Journal International*, 173, 49-62.

Zonge, K.L., (1994) *Vector IP (VIP) : A reconnaissance Approach*. Zonge Instruments.

**Tables**

Table 1. Results from the inversion of different data sets for the synthetic model.

| Data set | Number of data points | Data misfit (%) | Average % model misfit | Average resolution |
|---|---|---|---|---|
| Offset pole-dipole, single offset | 2868 | 1.21 | 3.12 | 0.0765 |
| Vector array, single offset (amplitude) | 2870 | 1.21 | 2.89 | 0.0726 |
| Vector array, double offset (amplitude) | 5138 | 1.24 | 2.20 | 0.0847 |
| Vector array, quadruple offset (amplitude) | 7842 | 1.42 | 2.39 | 0.0897 |
| Vector array, single offset (amplitude, direction) | 5740 | 1.20 | 2.57 | 0.0797 |
| Vector array, double offset (amplitude, direction) | 10276 | 1.23 | 2.07 | 0.0915 |
| Vector array, double offset (amplitude, direction) | 15684 | 1.42 | 2.24 | 0.0968 |

**Figure legends**
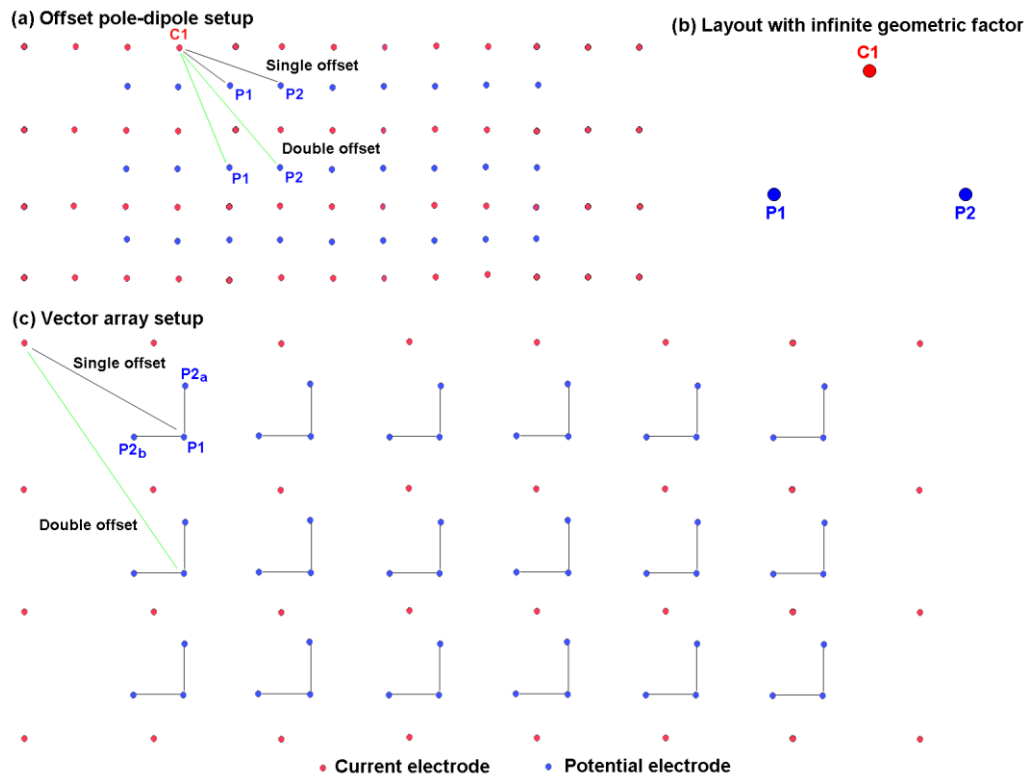
Figure 1. (a) Schematic diagram of electrodes layout for the offset pole-dipole survey. (b) An electrode array configuration with infinite geometric factor. (c) Schematic diagram for vector array survey electrodes layout.
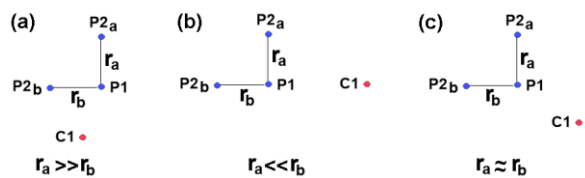
Figure 2. Variation of the resistance values measured by the potential dipoles of the vector array with orientation of the current electrode. (a) Very low potential signal at second dipole, (b) very low signal at first dipole, (c) signals with similar amplitudes at both dipoles.
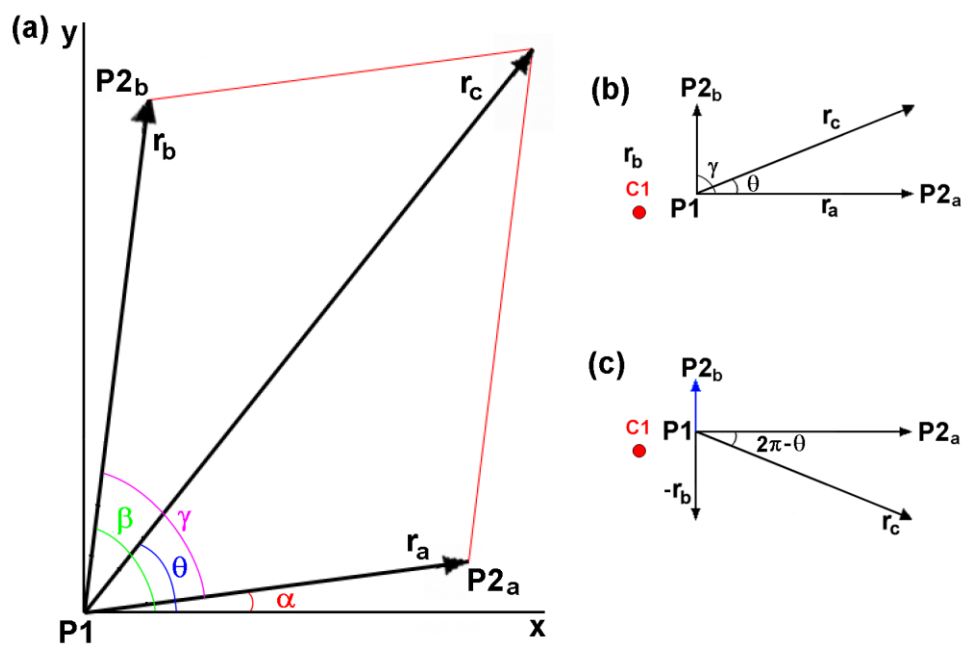
Figure 3. (a) Relationship of the amplitude and direction of the combined resistance value with the resistance values measured at the two potential dipoles of the vector array. Change of the direction of the combined resistance value with (b) small positive $r_b$ resistance, and (c) a small negative $r_b$ resistance value.
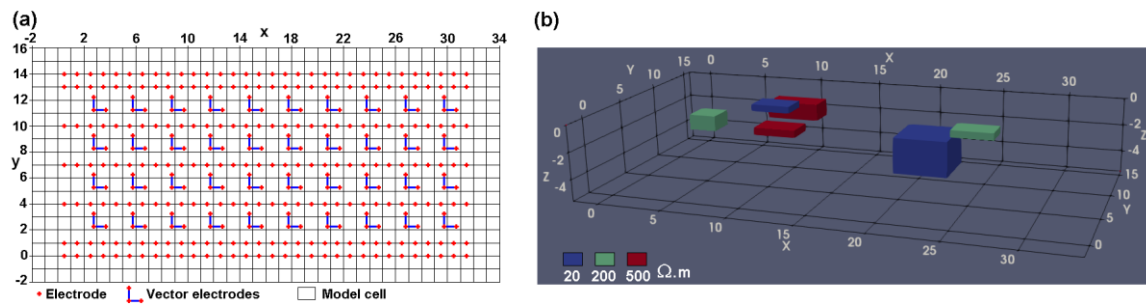
Figure 4. Synthetic data set model and survey configuration. (a) Arrangement of the current electrodes and potential triplets. (b) 3-D view of the synthetic test model. The background medium with resistivity of 50 Ω.m is transparent.
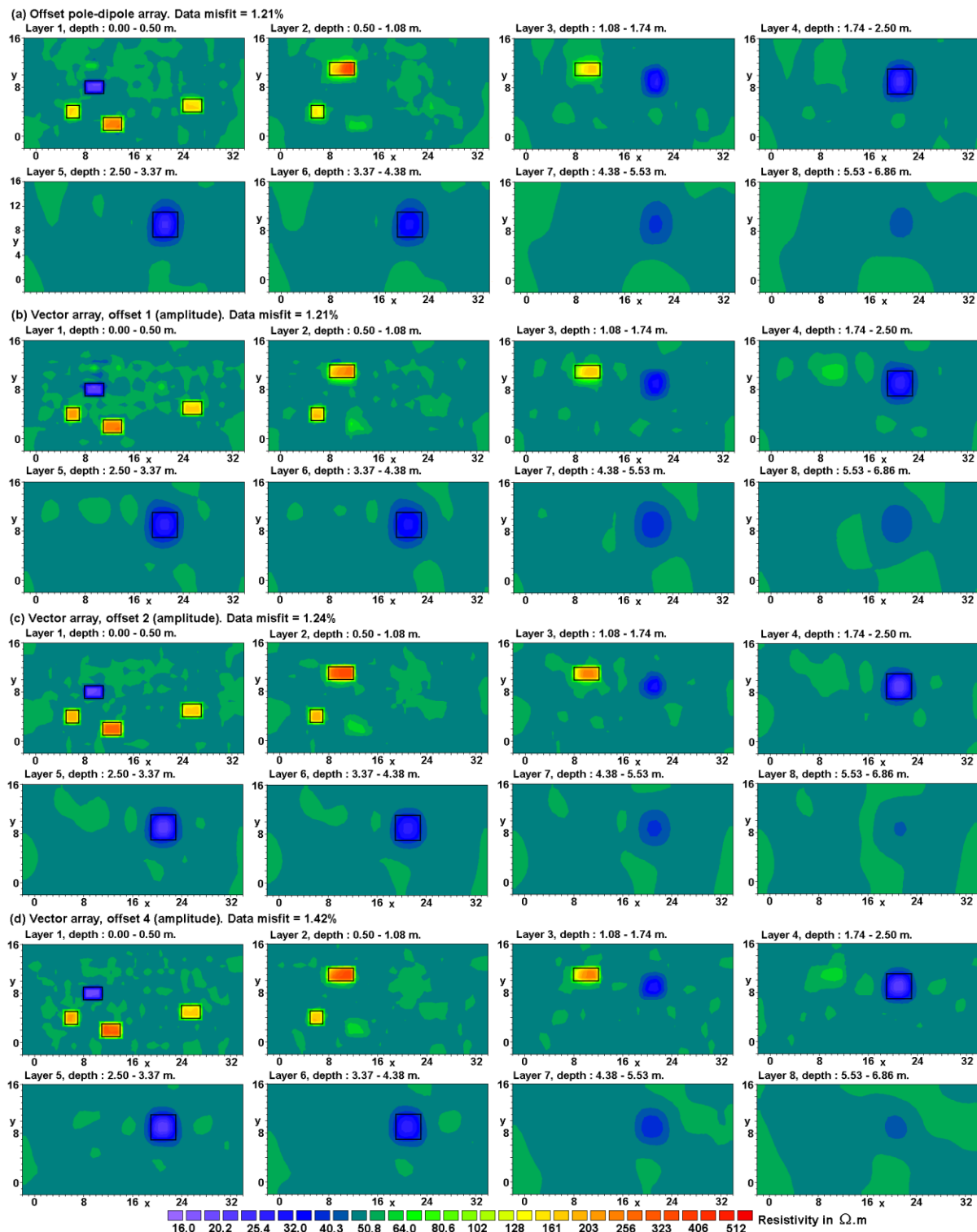
Figure 5. Inverse models for the (a) offset pole-dipole, (b) vector array with single offset of the potential electrodes, (c) vector array with double offset, (d) vector array with quadruple offset data sets. Only the amplitude component is used for the vector array data sets. The actual positions of the blocks are shown by black outlines.
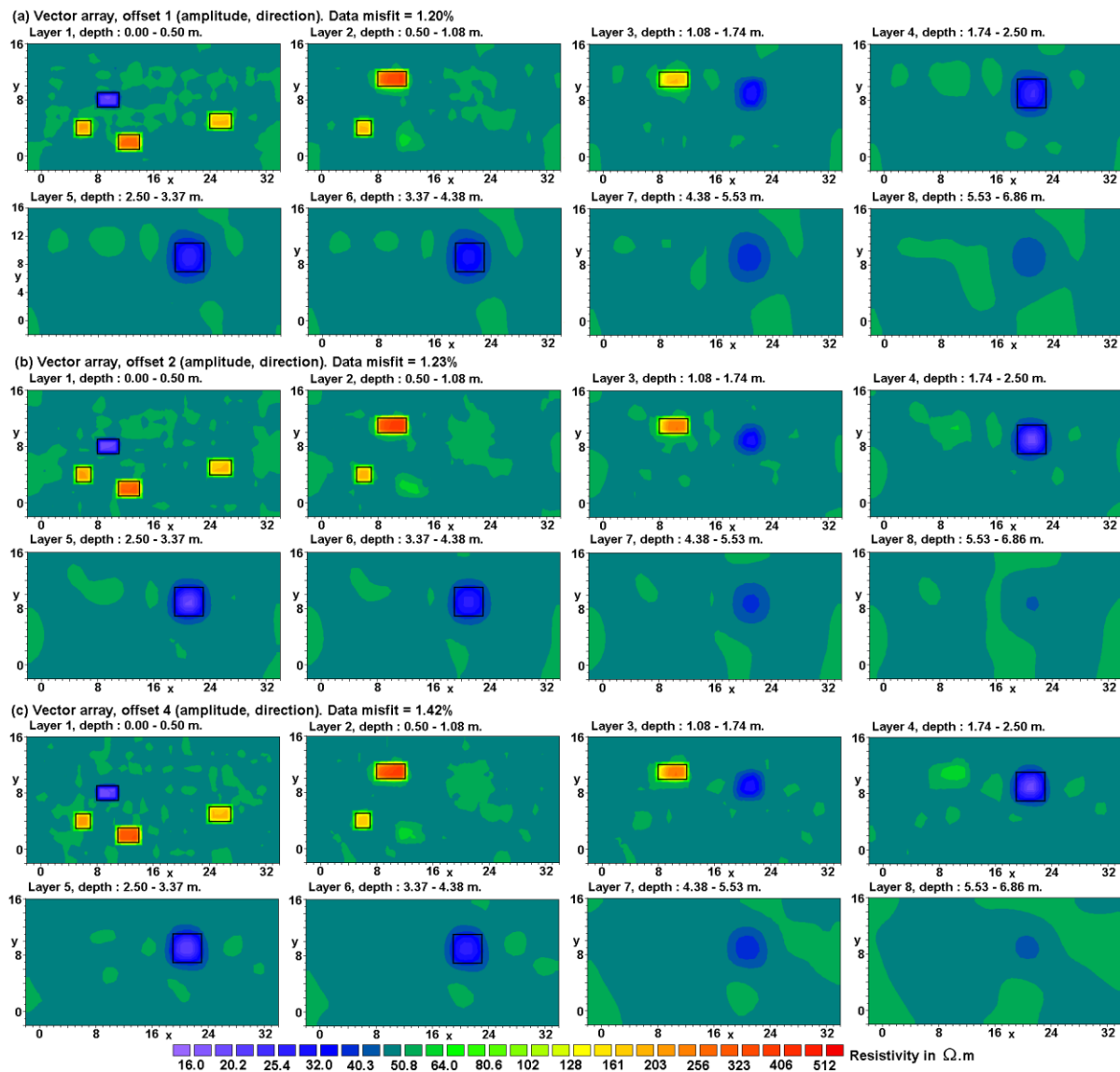
Figure 6. Inverse models for the (a) vector array with single offset of the potential electrodes, (b) vector array with double offset, (b) vector array with quadruple offset data sets. Both the amplitude and direction components are used in the vector array data sets. The actual positions of the blocks are shown by black outlines.
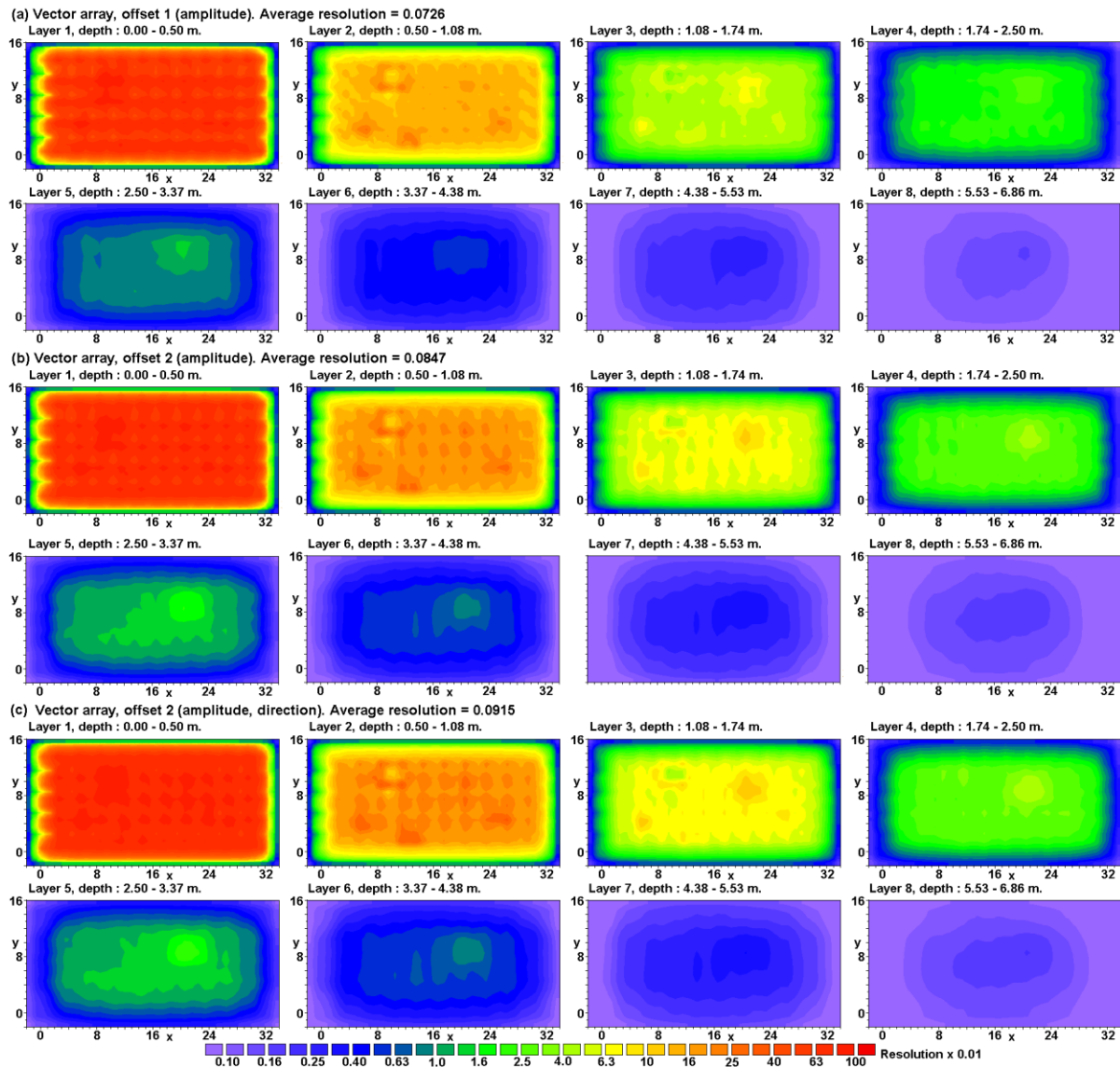
Figure 7. Model resolution sections for vector array data sets with (a) single offset of the potential electrodes and use of amplitude component only, (b) double offset with amplitude component only, (c) double offset with amplitude and direction components.
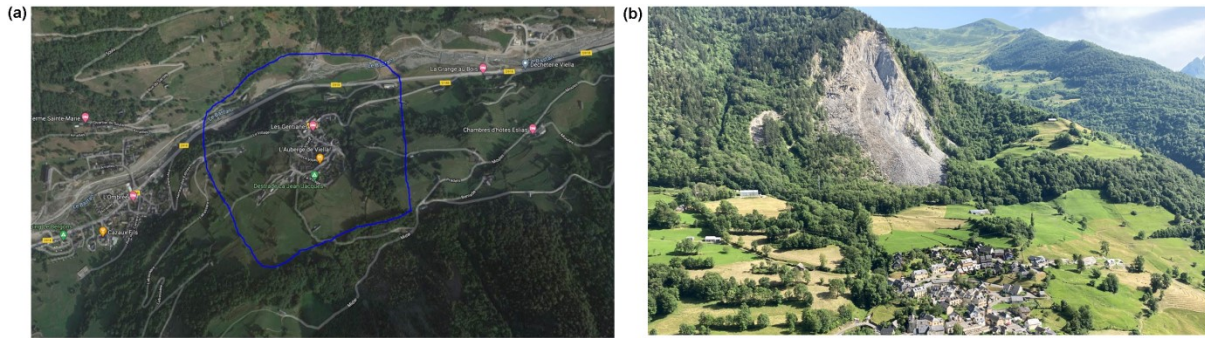
Figure 8. (a) Satellite map of centre of the survey area with the town of Viella. The blue line indicates the area covered by the survey electrodes. (b) Accumulation of rockfall debris above the deep low resistivity anomaly corresponding to the Viella landslide.
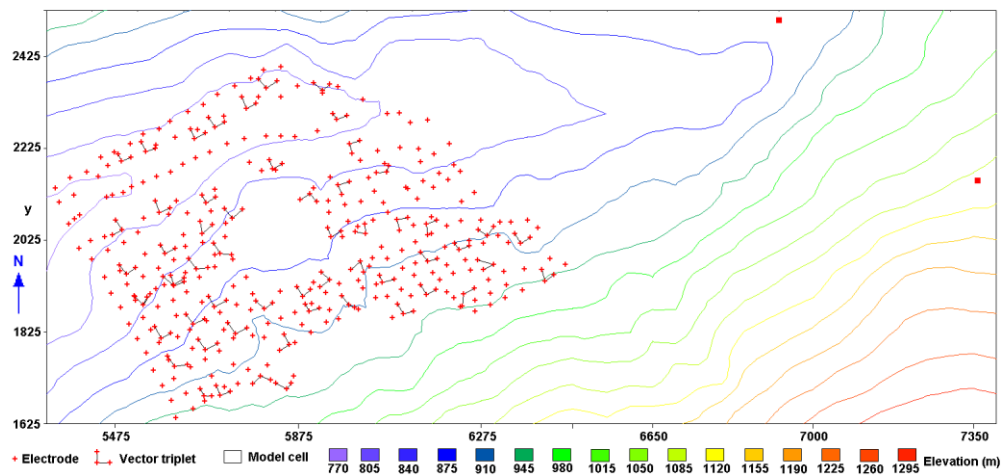
Figure 9. Plot showing the electrodes positions and topography in the survey area. The two

fixed remote electrodes are marked by red squares on the Eastern part of the plot.
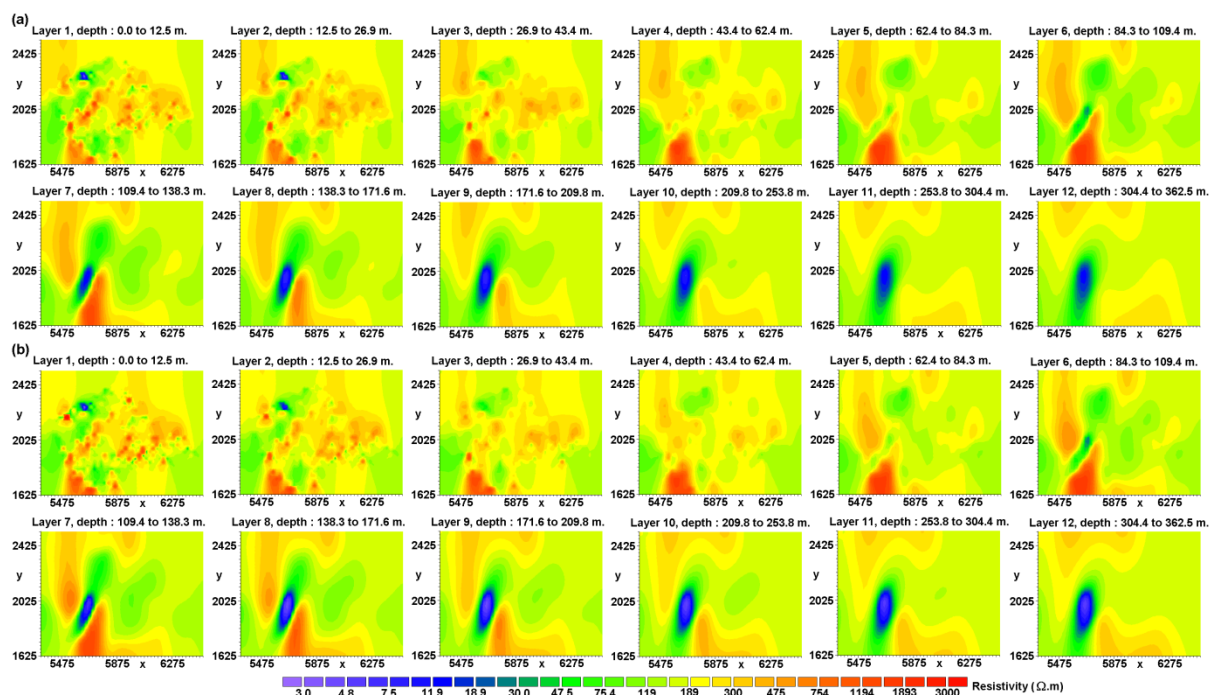
Figure 10. Inverse models obtained of the Viella landslide obtained (a) using amplitude component only (data misfit 10.2%), (b) including direction component (data misfit 9.1%). Only the Western part of the inverse model in the vicinity of the survey electrodes is shown. The model section between the edge of the survey area and the remote electrodes shows almost homogeneous resistivity values. The data set has 11115 vector array measurements.
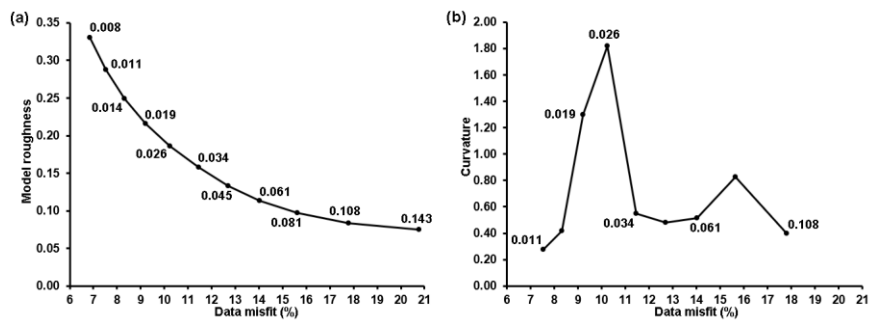
Figure 11. (a) L-curve showing change of model roughness versus the data misfit for inverse model obtained using different damping factors for the Viella data set. The damping factor values are shown next to the points on the curve. (b) Change of curvature of the L-curve with the data misfit.
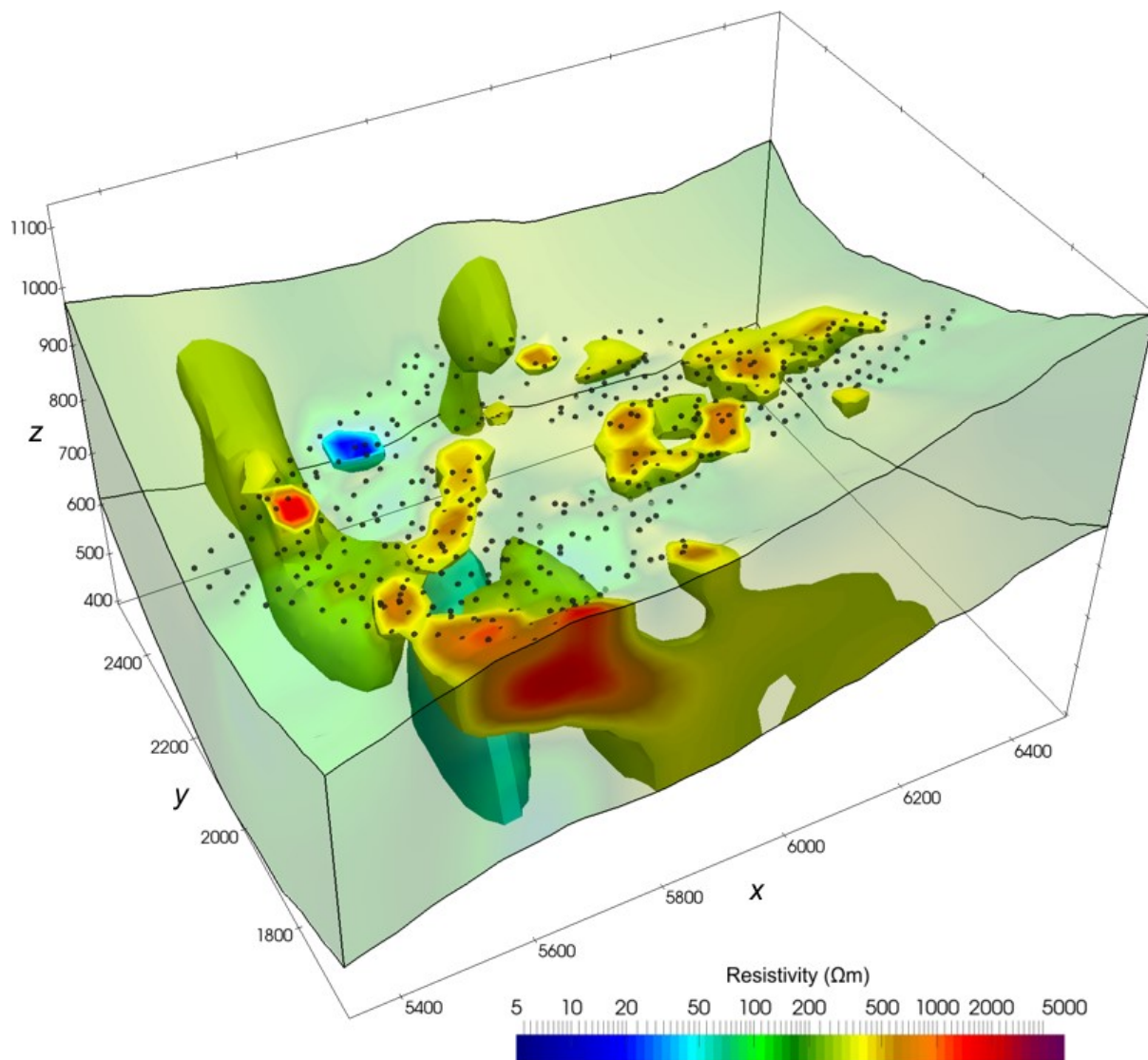
Figure 12. 3-D plot of Viella landslide inverse model (amplitude plus direction data) showing areas with resistivity of less than 50 Ω.m and greater than 300 Ω.m. The electrodes are marked by small dark circles.